Cold Cathode Fluorescent Lamps Driven by Piezoelectric Transformers: Stability Conditions and Thermal Effect

Sam Ben-Yaakov, *Member, IEEE*, and Mor Mordechai Peretz, *Student Member, IEEE*

***Abstract*—The envelope impedance (EI) concept was used to develop a systematic and simple approach for studying the conditions for stability of piezoelectric transformers (PT) based ballasts for cold cathode fluorescent lamps (CCFL) systems and the implications of the thermal operating conditions on such systems. The envelope analysis of the CCFL, which was verified experimentally, revealed that the magnitude of the negative EI decreases with temperature. This might cause the system to become unstable at low temperatures due to the fact that the loop gain of the PT–CCFL system encircled the $(-1, 0)$ point in the Nyquist plane. In such cases, the PT–CCFL system may enter a quasi-stable oscillatory operation mode in which the current is AM modulated by a low frequency parasitic signal. This phenomenon is analyzed and explained by considering the temperature effect on the EI of the CCFL. The results of this work provide an insight into the stability issue of the PT–CCFL system, and could help in finding remedies to the instability.**

***Index Terms*—Cold cathode fluorescent lamp (CCFL), envelope impedance (EI), piezoelectric transformer (PT).**

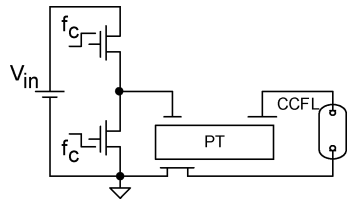

Fig. 1. PT-CCFL ballast system driven by half-bridge power stage.

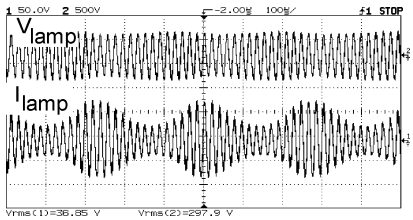

Fig. 2. Measured CCFL voltage (0.5 KV/div) and current (3.3 mA/div) when driven by a PT based HF electronic ballast. Horizontal scale 0.1 mS/div.

I. Introduction

PIEZOELECTRIC transformer (PT) based electronic ballasts for cold cathode fluorescent lamps (CCFL), such as the half-bridge (HB) inverter configuration of Fig. 1, were previously shown to be prone to instabilities [1]–[3]. Unstable operation may result in light flickering and extra voltage and current stresses, and in severe cases, may cause a runaway situation that will damage the lamp and the PT.

The stability condition of such PT–CCFL systems was examined in earlier studies by small-signal analysis and envelope simulation based on phasor transformation [1]–[4]. Still lacking, however, is an understanding of a number of phenomena related to this instability. For example, the reason that the system may be unstable at turn-on and then becomes stable after some warm up period. Another issue that needs clarification is the mechanism by which a PT–CCFL system, operating in open loop and driven by a constant frequency, will enter a stable oscillation condition with a constant modulation depth, as seen in Fig. 2. A possible explanation to these effects is a temperature dependence of the lamp's V–I curve that may cause a drift in the stability conditions of the PT–CCFL system.

In this study, we applied the envelope analysis and simulation concept to explore thermal effects on the operating conditions and the oscillation mechanism in PT based CCFL ballast systems.

Manuscript received February 14, 2006; revised May 26, 2006. This paper was presented in part at the IEEE Applied Power Electronics Conference (APEC), Dallas, TX, 2006 and at the Power Electronics Specialists Conference (PESC), Jeju, Korea, 2006. This work was supported by the Israel Science Foundation under Grant 113/02 and by the Paul Ivanier Center for Robotics and Production Management. Recommended for publication by Associate Editor J. M. Alonso.

The authors are with the Power Electronics Laboratory, Department of Electrical and Computer Engineering, Ben-Gurion University of the Negev, Beer Sheva 84105, Israel (e-mail: sby@ee.bgu.ac.il).

Digital Object Identifier 10.1109/TPEL.2007.896446

II. "Envelope Impedance" Concept

To illustrate the importance of envelope behavior of the PT–CCFL system, we first consider the case of a CCFL driven by a conventional HF ballast (Fig. 3). Assume that $V_{\rm in}$ (Fig. 3) is an adjustable ac source that keeps the rms lamp current constant. By this, the lamp will always be at the same rms operating point. Consider now two cases, one in which the source frequency is very high and the other in which the source frequency is close to the resonance of L_s, C_s. It is clear intuitively and observed experimentally that the system will be stable when driven at very high frequency but unstable when driven at a frequency that is close to the (L_s, C_s) resonant frequency, f_r. This is because at high frequency, the CCFL sees a current source (high impedance of the inductor) while at the resonant frequency it sees a voltage source, which will render the system unstable [5]. This virtual experiment shows

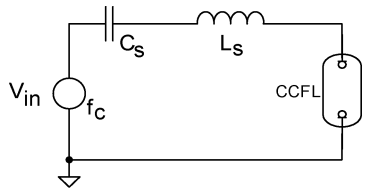

Fig. 3. CCFL driven by a HF resonant ballast.

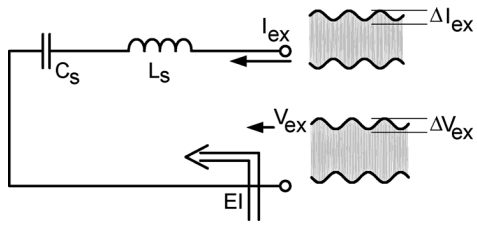

Fig. 4. Illustrative explanation of the envelope impedance (EI) concept: EI $(f) = \{\Delta V_{\rm ex}/\Delta I_{\rm ex}\}(f)$.

that in the case of nonlinear carrier-driven systems, stability is not just a network attribute but it depends on the carrier frequency. That is, the same system will be stable for one carrier frequency but unstable for another. This is in contrast to linear feedback systems in which stability is a characteristic of the system and independent of the excitation. Furthermore, in this case, stability conditions are not only dependent on the magnitude of the excitation (which sets the operating point) but also on the frequency of the carrier. For the given example, the crucial stability parameter is the envelope impedance (EI) [5], [6] that is defined here as the ratio of the envelope of the voltage ($\Delta V_{\rm ex}$), to the envelope of the current ($\Delta I_{\rm ex}$), when the network is driven by an AM modulated signal, $V_{\rm ex}$ (Fig. 4).

It should be noticed that the EI is, in general, a complex number, that is a function of the modulating signal frequency, f_m, and the carrier frequency, f_c. The carrier frequency can be considered in this case as the "bias point," whereas the modulating frequency, f_m, as the "signal frequency."

Following the above intuitive observation, we consider next the nature of the EI for the example on hand, the resonant ballast of Fig. 4. When the network is driven by an AM modulated signal, the signals involved are the carrier frequency (f_c) and the two side bands: $(f_c - f_m)$ and $(f_c + f_m)$. For a given network with a resonant frequency f_r, the expected EI as a function of the modulating frequency f_m, for a given carrier frequency f_c, can be guessed by considering the plot of Fig. 5. It shows the impedance of the resonant network (Z_b) as a function of frequency, the location of the carrier frequency f_c and the frequencies of the sidebands. Fig. 5 implies that when $f_m = |f_c - f_r|$ one would expect to see a valley in the EI. It should be noticed that the valley is located at a frequency that could be substantially lower than f_c or f_r.

III. Stability Criterion

Following [5], we can consider the PT-CCFL system operating in open loop (Fig. 6) as a feedback system (Fig. 7).

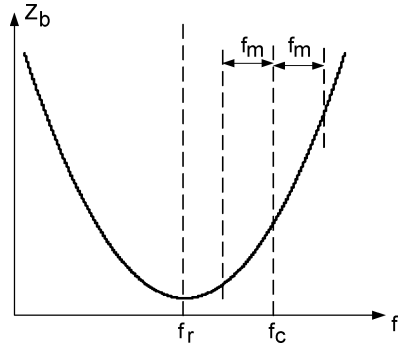

Fig. 5. Impedance of a series resonant network, a carrier frequency, and side bands.

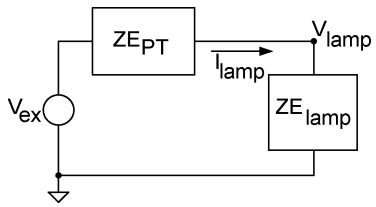

Fig. 6. Simplified PT–CCFL ballast system.

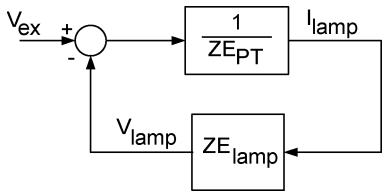

Fig. 7. PT–CCFL ballast system represented as a feedback loop.

It should be noticed that the relevant impedances of both elements are their envelope impedances (EI) [5]. The stability of the PT–CCFL system can thus be studied by analyzing the loop gain (LG) of the feedback loop of Fig. 7 [5]

$$\mathrm{LG}\,(T) = \frac{\mathrm{ZE_{CCFL}}\,(T)}{\mathrm{ZE_{PT}}} \tag{1}$$

where $\mathrm{ZE_{PT}}$ is the output EI of the PT and $\mathrm{ZE_{CCFL}}$ is the EI of the lamp which is already assumed here to be a function of temperature T.

Equation (1) implies that instability is reached when the EI ratio will encircle the $(-1, 0)$ point in the Nyquist plane. This will occur if

$$\left|\frac{\mathrm{ZE_{CCFL}\,(T)}}{\mathrm{ZE_{PT}}}\right| \geq 1 \tag{2}$$

when the phase of LG, φ(LG), is (-180°).

IV. EI of the PT and the CCFL

Envelope impedances do not obey, in general, Kirckhoff Laws. In particular, the EI of two networks in parallel may not be equal to the equivalent EI value calculated by conventional phasor analysis, from the individual EIs. It can be shown though, that in the private case of a resistor that is in parallel

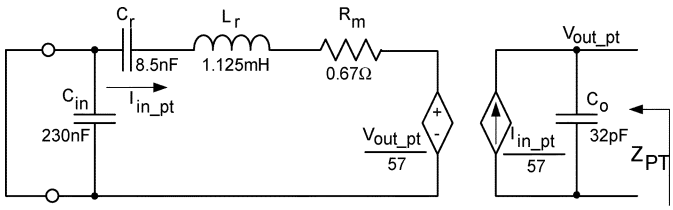

Fig. 8. PT equivalent circuit and parameters, connected in the output impedance measurement setup.

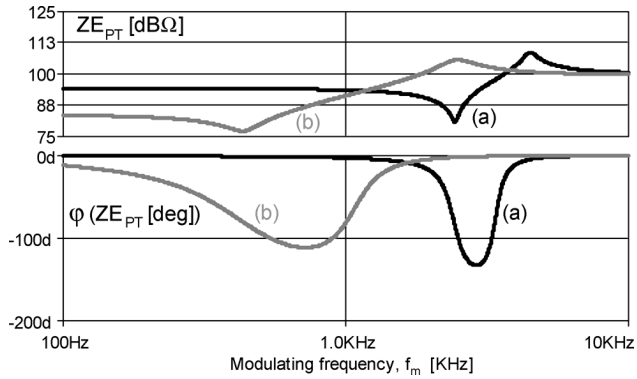

Fig. 9. Envelope Impedance of experimental PT (ELECERAM ELM-610) for two carrier frequencies:(a) operation far from output impedance resonance of the PT $f_c = 49$ KHz and (b) operation near resonance $f_c = 51$ KHz ($f_r = 51.5$ KHz).

with a general EI, the conventional analysis still applies. That is, the total envelope admittance of the combined network can be obtained by adding the conductance of the resistor to the real parts of EI's admittance. This observation is the justification to the approximate stability analysis method that is proposed below, in which the behavior of the complete PT-CCFL system is examined by considering separately the EIs of the PT and CCFL. This issue is further discussed in Section VII below, in conjunction with Nyquist plots of the system.

A. EI of a PT

Applying the one-mode equivalent circuit of a PT (Fig. 8) one can reach an intuitive insight of the expected EI by considering the fact that an AM modulated signal includes two side bands: $(f_c - f_m)$ and $(f_c + f_m)$. On the other hand, the output impedance of a PT is expected to reach a minimum value for frequencies near the mechanical resonance f_r emulated by L_r and C_r in Fig. 8. Consequently, one would expect to see a minimum value in the output EI of the PT, $\mathrm{ZE_{PT}}$, when $f_m \cong |f_c - f_r|$. A convenient way to obtain $\mathrm{ZE_{PT}}(f_m)$ for a given carrier frequency f_c is by envelope simulation [7]–[10]. A typical EI plot (of experimental PT) is shown in Fig. 9. The plot can be better understood by comparing it to the (conventional) output impedance of the PT (Fig. 10). The comparison between the plots shows that the minimum values of the EI in Fig. 9 are located at modulating frequencies of 2.5 KHz and 0.5 KHz which are equal to the difference between the carrier frequencies (49 and 51 KHz, respectively) and the resonant frequency: 51.5 KHz.

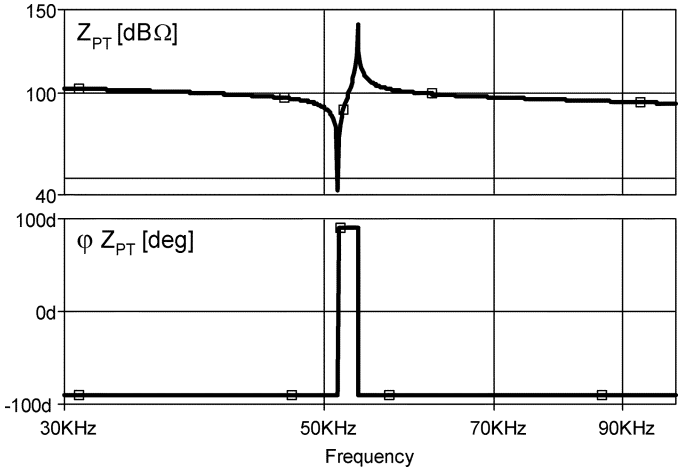

Fig. 10. Output impedance of experimental PT.

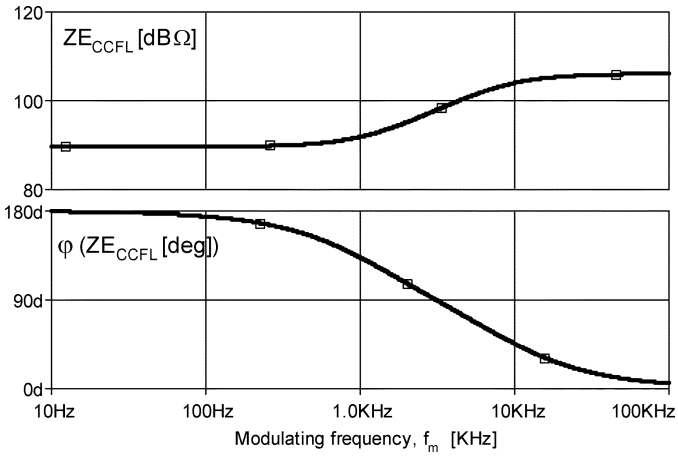

Fig. 11. Envelope Impedance of experimental CCFL (JKL BF3250–20B).

B. EI of a CCFL

Earlier studies have shown [5], [11], [12] that the EI of a CCFL driven by a high frequency carrier f_c, $\mathrm{ZE_{CCFL}}$, can be expressed as a function of the modulating frequency f_m as

$$\mathrm{ZE_{CCFL}}(T) = R_s(T)\,\frac{\frac{jf_m}{f_p}\cdot\frac{R_{\mathrm{eq}}(T)}{R_s(T)} - 1}{\frac{jf_m}{f_p} + 1} \tag{3}$$

where $R_{\mathrm{eq}}(T)$ is the ac resistance of the lamp at the given operating point for the f_c excitation, $R_s(T)$ is a constant of the lamp obtained from a static set of V–I measurements of the CCFL [11], all assumed to be temperature dependent. The relaxation time of the lamp's plasma $[1/(2\pi \cdot f_p)]$ was considered, as first approximation for the experimental conditions of this study, to be independent of the temperature (will be discussed in the experimental section below).

A convenient way to plot $\mathrm{ZE_{CCFL}}$ is by running a simulation on a behavioral model of the CCFL [5], [11]. A typical EI plot (of the experimental CCFL), which supports the results of (3), is depicted in Fig. 11. It shows that at low modulating frequencies $(f_m < f_p)$ $\mathrm{ZE_{CCFL}}$ is negative (constant amplitude and angle of 180°), approaching $(-R_s)$ at $(f_m \to 0)$ while at high

frequencies ($f_m \rightarrow \infty$) the EI becomes positive (constant amplitude and angle of 0°).

V. Stability of PT-CCFL System

Considering the above observations, the ratio of $\mathrm{ZE_{CCFL}}$ to $\mathrm{ZE_{PT}}$ (1) may indeed reach, at low frequencies, a phase shift of -180°. The ratio will be larger than -1 (1) if

$$|\mathrm{ZE_{CCFL}}(T)| > |\mathrm{ZE_{PT}}|. \tag{4}$$

That is, the system will be unstable when the absolute value of the negative EI of the CCFL is larger than the positive EI of the PT. As pointed out earlier, $\mathrm{ZE_{PT}}$ is expected to have a minimum for $f_m \cong |f_c - f_r|$. Hence, for operation at the same frequency range, the system will be unstable if the EI of the CCFL exhibits a large negative resistance value.

VI. Experimental

A. Extraction of the PT Model Parameters

The PT was a multilayer Rosen type transformer (ELECERAM ELM-610). The objective of the parameter extraction procedure was to estimate the values of the elements of the PT equivalent circuit (Fig. 8) around the operating frequency of the element (53 kHz) and under nominal applied voltage and load conditions. Parameter extractions by impedance or network analyzers are normally carried out under low voltage and low power conditions. This may lead to large errors since piezoelectric elements are nonlinear devices and their parameters are expected to vary as a function of the applied voltage and loading [13], [14]. Thus, in this study, the parameters extraction approach adopted is similar to the one described earlier [15] for extracting the terminal impedance of a piezoelectric resonant blade. The difference between the procedure used here and the earlier one is the number of parameters that need to be extracted. In the PT case, two extra parameters are included in model: the transfer ratio of "transformer" (the two coupled dependent sources) and the output capacitance (C_o, Fig. 8). The extraction procedure was based on some advanced PSpice (Cadence, USA) Version 10 features: a frequency domain data-driven behavioral source (EFREQ), and the PSpice optimization tool.

1) Reference Measurement: The first stage of the extraction procedure was measuring the input to output transfer ratio (TR) of the PT. This was done, in present work, by a network analyzer (HP4395A) coupled to a power amplifier to allow high voltage excitations [13] (Fig. 12). The input resistance of the network analyzer used in this study (HP4395A) is 50 Ω (probes A and R of Fig. 12) with a maximum input voltage of 1 V. Thus, to facilitate high voltage measurements, voltage dividers were applied at the input and output of the PT ($R_{\mathrm{trm}} = 2.2$ KΩ, and R_{load}–load resistance, 100 KΩ nominal, Fig. 12). The measurements results were saved as a table file that includes the information of magnitude and phase for each frequency point over the measurement range (48 to 60 KHz) that was chosen to be around the peak of TR response.

2) Emulating the Measurement in PSpice: The table obtained from the TR measurement was inserted into a PSpice EFREQ behavioral dependent source [15] (Fig. 13) to create a

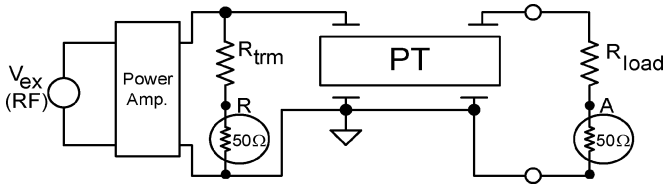

Fig. 12. Experimental setup for input to output voltage transfer ratio measurements. The ratio A/R was measured by a network analyzer (HP4395A). The 50 Ω resistors represent the input resistance of the network analyzer.

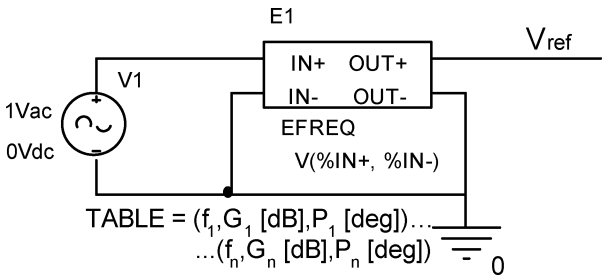

Fig. 13. PSpice emulator of experimental TR of the PT. The table of the EFREQ dependent source lists the measured TR (magnitude and phase) over the measured frequency range.

subcircuit that emulates the measured TR of the PT. This source generates a voltage that is a function of a PSpice 'expression' multiplied by a discrete table defined in the frequency domain. In present case, the 'expression' of the EFREQ (Fig. 13) is $(V(\%\mathrm{IN}+, \%\mathrm{IN}-))$, which denotes the input voltage to the element. When a unity ac voltage source is fed to this behavioral source, its output voltage will duplicate the measured TR of the experimental PT.

3) PSpice (Cadence) Optimization Tool [16]: This add-on package allows the selection of the values of some circuit components to meet a specific goal function. The initial data that are fed to the optimizer include expression of the goal function, additional constraints, if any, and initial values of the components to be optimized.

The objective of the optimization procedure used in this study was to find values of the parameters depicted in Fig. 8 such that they would faithfully represent the experimental PT. This was accomplished by running a set of ac simulations that include the equivalent PT model (Fig. 8) and the EFREQ (Fig. 13), each fed by a unity ac voltage source, and letting the optimizer choose the values of the PT model that will minimize a least square error function. The "err" goal function was defined by

$$\mathrm{err} = [\mathrm{dB}(V_{\mathrm{ref}}) - \mathrm{dB}(V_{\mathrm{mod}})]^2 \times 100 + [P(V_{\mathrm{ref}}) - P(V_{\mathrm{mod}})]^2. \tag{5}$$

The fitting objective

$$1 \leq \mathrm{err} \leq 10$$

for

$$50\ \mathrm{KHz} \leq f \leq 56\ \mathrm{KHz}$$

where "dB" and "P" designate decibel and phase operators, respectively, V_{ref} is the output voltage of the EFREQ behavioral source (V_{ref}, Fig. 13) and V_{mod} is the output voltage of the PT

TABLE I
DATA EXTRACTED FROM SC IMPEDANCE MEASUREMENTS THAT WAS FED, AS INITIAL DATA, TO THE OPTIMIZER

C_{in}	L_r	C_r	R_m	C_o	N
141nF	1.19mH	7.9nF	1.125Ω	26pF	49

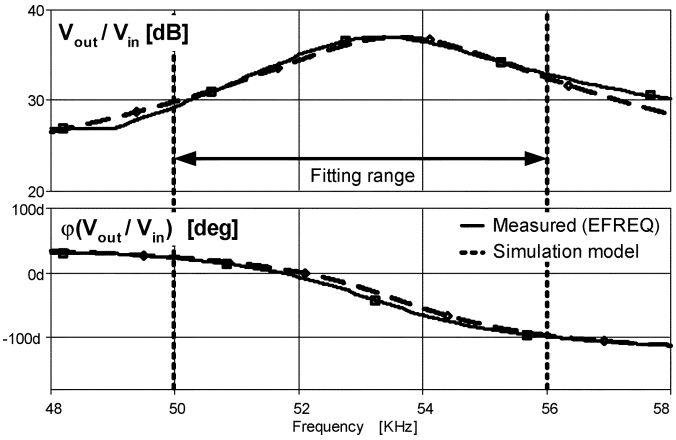

Fig. 14. Comparison between measurement result (solid) and optimized model (dashed) input to output TR of experimental PT.

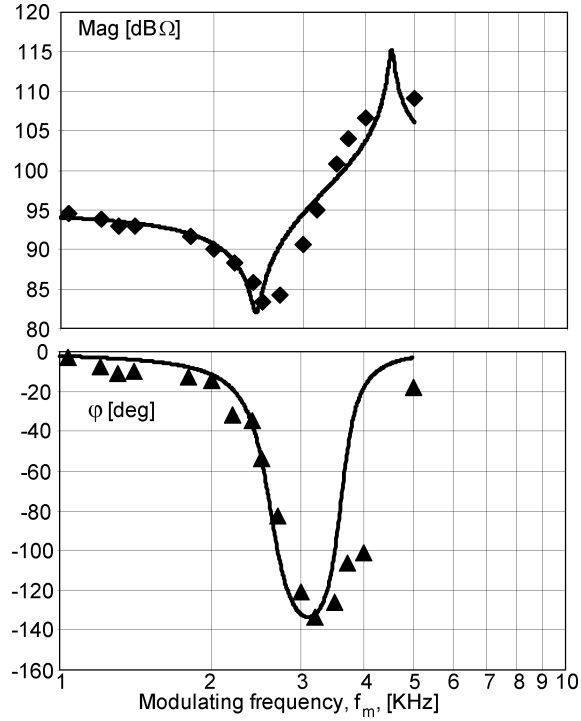

Fig. 15. Measured (symbols) and simulated (solid lines) magnitude and phase EI of experimental PT (ELECERAM ELM-610). Carrier frequency: 49 KHz, resonant frequency: 51.5 KHz.

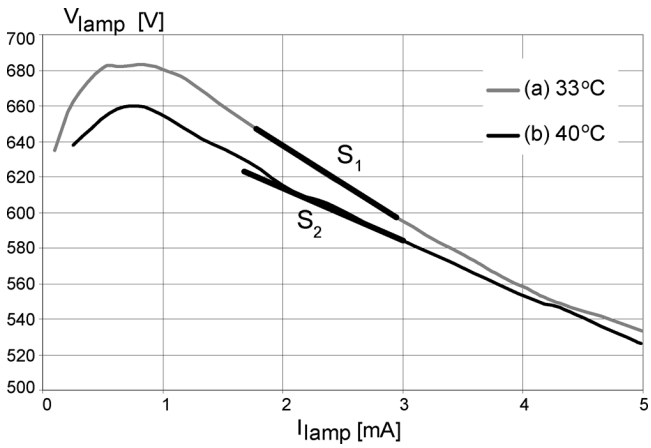

Fig. 16. Measured static V–I curves of experimental CCFL (JKL BF3250–20B) operating in two thermal bias points: (a) 33 °C. (b) 40 °C.

model ($V_{\text{out\_pt}}$, Fig. 8). The 100 gain enhancement factor in (5) is used to increase the sensitivity of the error function to gain discrepancies. The limits of the "err" goal function were selected to avoid convergence problems on one hand (hence, err>=1) and on the other hand, to ensure sufficient accuracy (err<=10). Both the gain enhancement factor and error limits were selected through a series of trial and error simulation.

The fitting was carried out around a narrower frequency range (50 to 56 KHz) to improve the accuracy near the TR peak. The initial values of the model components, needed as an input to the optimization routine, were obtained from two short-circuit (SC) impedance measurements at low applied voltage (input SC and output SC). The parameters of the SC measurement were extracted by the fitting routine imbedded in the analyzer, using the HP16092A impedance test kit that was connected to the HP4395A network analyzer. The initial data that were fed to the optimizer are given in Table I.

The estimated values of the PT's model parameters are given in Fig. 8, and the comparison between the measured TR (EFREQ) and model calculated (optimized) TR is depicted in Fig. 14. The observed discrepancies are probably due to the nonlinear nature of the PT, when driven by high voltage excitations [13]. However, these differences are negligible within the frequency range (50 to 56 KHz) of interest.

An experimental measurement of the PT's EI was taken at a carrier frequency of 49 KHz, 2.5 kHz off the resonance frequency of the PT ($f_r = 51.5$ KHz). The EI measurement was carried out by subjecting the PT to an AM modulated signal at the output while its input terminals were short circuited. The EI (magnitude and phase) was measured as a function of the modulating frequency (f_m from 0 to 5 KHz). The measured EI (Fig. 15) has its minimum at 2.5 KHz, which is exactly the frequency difference between f_c and f_r. The results are in a very good agreement (magnitude and phase wise) with the envelope simulation (Fig. 15) that was carried out on the PT model using the parameters values that extracted by the proposed procedure.

B. CCFL Model Extraction Procedure

The experimental CCFL (JKL BF3250–20B) was of 3.2 mm diameter, 250 mm long, 5 mArms nominal current and 520 Vrms nominal voltage. The static V–I curves of the experimental lamp were measured for two lamp temperatures and are given in Fig. 16. This was accomplished by cooling the lamp using air ventilation with two 220 V/17 W fans. The lamp surface temperature was monitored by thermaCAM E45 (FLIR systems) infrared thermal camera. The recorded data were then used to extract the parameters of the lamp SPICE-compatible model (Fig. 17) [5], [11].

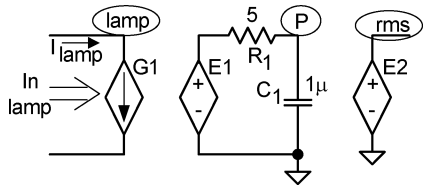

Fig. 17. CCFL behavioral model.

In this model the lamp is represented as a dependent current source (G_1, Fig. 17) that emulates a variable resistance

$$\mathrm{G1}\,(33\,^\circ\,\mathrm{C}) = \frac{V(\mathrm{lamp})}{\frac{723}{V(\mathrm{rms})} + 1.13\cdot 10^6\cdot V(\mathrm{rms}) - 45\cdot 10^3} \quad (6)$$

$$\mathrm{G1}\,(40\,^\circ\mathrm{C}) = \frac{V(\mathrm{lamp})}{\frac{690}{V(\mathrm{rms})} + 1.13\cdot 10^6\cdot V(\mathrm{rms}) - 38.6\cdot 10^3} \quad (7)$$

where $V(\mathrm{lamp})$ is the lamp rms voltage, and $V(\mathrm{rms})$ is a voltage that emulates the rms lamp current. The denominators of (6) and (7) represent the CCFL equivalent resistance curve at a given thermal operating conditions (33 °C and 40 °C, respectively). This data were obtained by fitting the template of (6) and (7) to the static lamp resistance derived from the measured V-I curves of Fig. 16 [11] at the corresponding thermal bias point.

The output of the dependent voltage source E_1 (Fig. 17) is proportional to the square of the lamp current $\{i(\mathrm{lamp})\}$

$$E_1 \equiv \{i(\mathrm{lamp})\}^2. \quad (8)$$

The output voltage of E_1 is then passed thru a low-pass network (R_1, C_1, Fig. 17) to extract the low frequency components [5]. The average voltage of C_1 (node "p" in Fig. 17) is thus a smoothed value of the square rms current. The filtered rms current is then obtained by E_2 (node "rms" in Fig. 17) as the square root of $V(p)$

$$E2 = \sqrt{V(p)}. \quad (9)$$

The time constant R_1C_1 is chosen by matching the envelope response of the model to experimental results. This was done, in the present study, by subjecting the PT-CCFL system to a HF carrier that was FM modulated. This caused an AM modulated signal at the lamp terminals due to the PT equivalent series inductance (L_r, Fig. 8) [6], [17]. The CCFL current and voltage traces were then recorded at two thermal bias points for several modulating frequencies to obtain its EI.

The time constant R_1C_1 (Fig. 17) is then adjusted to match the model simulated results to the measured response. Fig. 18 shows the measured EI of the experimental CCFL under two thermal operating conditions, compared with the results of the CCFL SPICE model of Fig. 17. Notice that $|\mathrm{ZE_{CCFL}}|$ decreases with the rise of T, however, the phase $\varphi(\mathrm{ZE_{CCFL}})$ approximately maintains the same frequency response. This implies that the relaxation time of the lamp's plasma can be considered, as first approximation, independent of the temperature for the experimental conditions. The results of the simulated EI of Fig. 18 were obtained by first extracting the time constant using the set of measurements at 33 °C and then running the model for

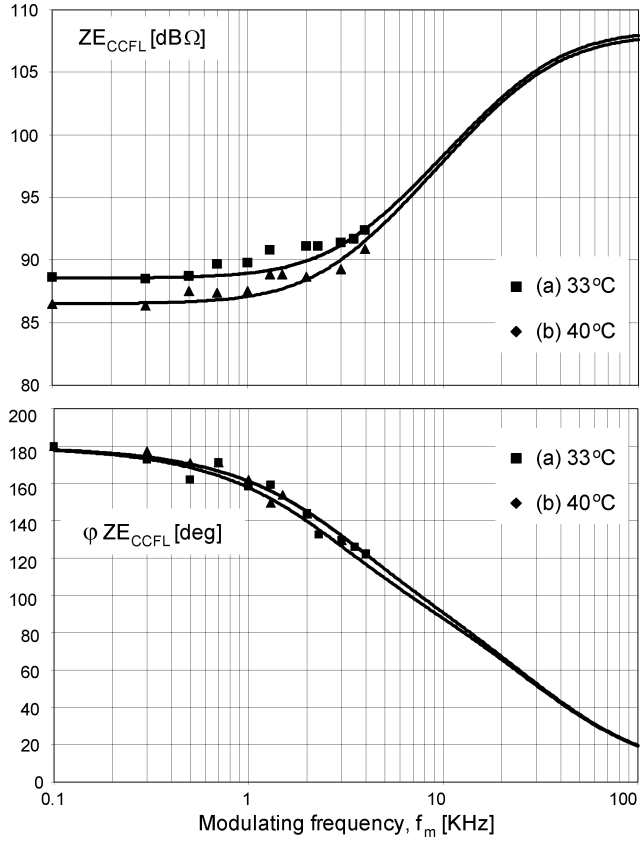

Fig. 18. Measured (symbols) and simulated (solid lines) magnitude and phase EI of experimental CCFL (JKL BF3250–20B) in two thermal bias points: (a) 33 °C and (b) 40 °C.

TABLE II
CCFL MODEL PARAMETERS OF TWO THERMAL OPERATING CONDITIONS AT LAMP CURRENT OF 3 mA

T @3mA	R_{eq} @3mA	R_s @3mA	f_p
33°C	199.4 KΩ	-38.26 KΩ	200 KHz
40°C	194.79 KΩ	-31.26 KΩ	200 KHz

thermal bias point of 40 °C [the current source G1 of Fig. 17 is changed according to (7)]. From the denominators of (6) and (7), which represent the fitted R_{eq} of the lamp at the two temperatures, one can obtain the CCFL ac resistance [R_{eq}, (3)] at any lamp current within the measurement range. R_s (3) is the local slope of the V–I curve and hence can also be calculated from the measured V–I data. At 3-mA lamp current, for which the stability analysis was carried out (see Section VII below), the R_{eq}, R_s and the fitted relaxation frequency f_p, are summarized in Table II.

VII. RESULTS AND DISCUSSION

A very good agreement was found between the measured $\mathrm{ZE_{CCFL}}$ and the simulated one which verified the validity of the lamp model. The relatively large scatter of the measured value is probably due to the fact that under the experimental conditions the voltage envelope of the lamp was very small. The data obtained from the small-signal envelope simulations of the PT and the CCFL were than used to generate Nyquist plots of the PT-CCFL LG for two carrier frequencies (49 and 51 KHz) and two temperatures (33 °C and 40 °C) (Fig. 19). The Nyquist plots

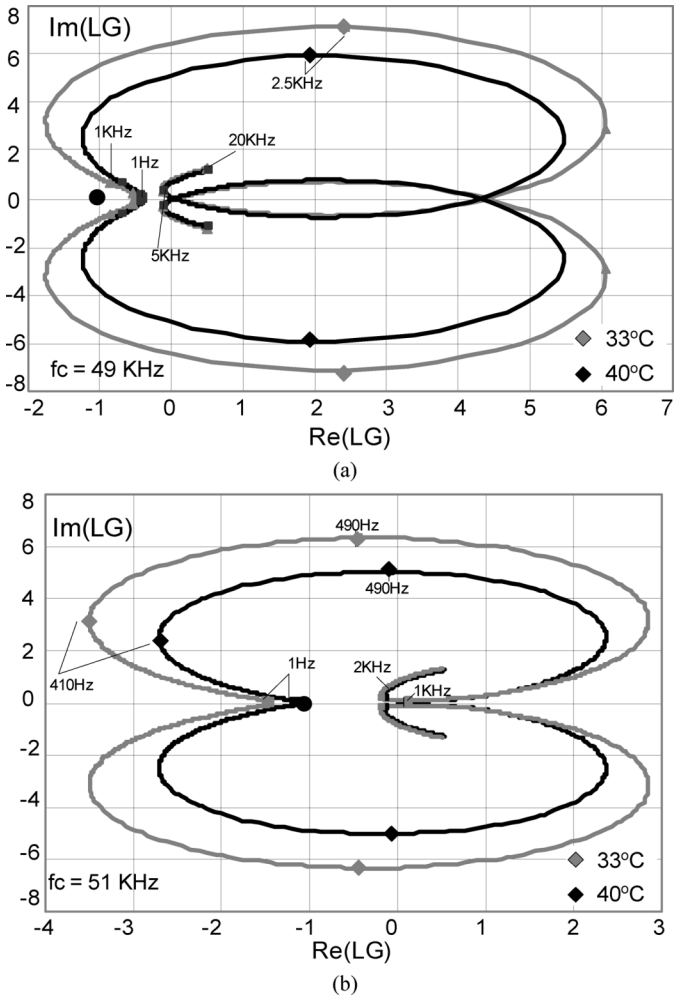

Fig. 19. Nyquist plots of experimental PT-CCFL system under different operating conditions (carrier and thermal wise): (a) carrier frequency is far from resonance, stable operation in both thermal operating points and (b) carrier frequency near resonance, 40 °C: stable operation, 33 °C: unstable operation.

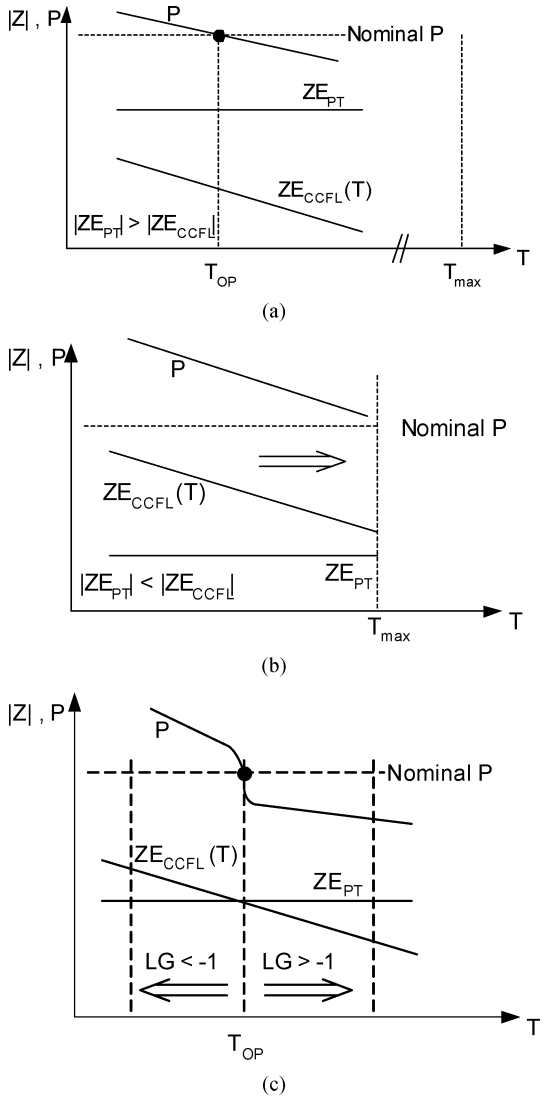

Fig. 20. Possible modes of operation of PT-CCFL system: (a) f_c far from f_r, stable mode and (b) $f_c = f_r$ unstable mode and (c) f_c near f_r, oscillations mode.

of Fig. 19(a) show stable operation of the PT–CCFL system when driven by a carrier that is far from the PT's resonance, however, when f_c is close to f_r, the Nyquist test of Fig. 19(b) predict unstable operation for 33 °C and stable operation for 40 °C—as observed experimentally.

As pointed out earlier, the EI of two networks in parallel may not be equal to the equivalent EI value calculated by conventional phasor analysis. Consequently, the Nyquist plots of Fig. 19 may be in error. However, for the part of the plots that is crucial to the stability criterion, the error may be negligibly small. The reason for that is the fact that the circling, or not circling, of the (-1) point is determined by the extreme left point of the Nyquest plot (Fig. 19). As it turns out, this part of the plots is related to the low modulation frequency region of the $\mathrm{ZE_{CCFL}}$ where the lamp can be considered a pure negative resistance (Fig. 11). In the special case of a system that is composed of a pure resistor and a complex EI, the total EI can be evaluated by combining the effects of each individual part, as done in conventional network analysis. This observation is based on numerous simulation runs but has not been proven rigorously as yet. Based on this conjecture, the Nyquist stability criterion can still be applied even though the ratio of $\mathrm{ZE_{CCFL}}/\mathrm{ZE_{PT}}$, where each was individually evaluated, may not be exactly equal to the system's LG.

The reason for the unstable operation at 33 °C is explained by the fact that absolute magnitude of the negative R_s (33 °C) is larger than R_s (40 °C) (local slope of the V–I curves shown in Fig. 16), sufficiently large to satisfy (4).

The thermal effect on the operation of the PT-CCFL system can be explained by considering three possible modes of operation, taking into account the difference between f_c and f_r. When f_c is far from f_r [Fig. 20(a)], $\mathrm{ZE_{CCFL}}$ will be smaller than $\mathrm{ZE_{PT}}$, the lamp will work at its nominal power (P) range and the system is stable. When f_c is approximately equal to f_r [Fig. 20(b)], $\mathrm{ZE_{PT}}$ will have a minimum at very low modulating frequency (Fig. 9) where $\mathrm{ZE_{CCFL}}$ is negative, causing the system to be highly unstable. This will cause the lamp current to build up and the system will enter a runaway condition. This operation mode is unsafe from a practical point of view since that the high rms current due to the unrestrained oscillation will

cause excessive heat that will eventually damage the CCFL. The third mode of operation will occur at carrier frequencies that are near f_r causing a moderate instability, that is, LG is slightly more negative than -1 [Fig. 20(c)]. In this mode $\mathrm{ZE}_{\mathrm{CCFL}}$ intersects with $\mathrm{ZE}_{\mathrm{PT}}$ at a given thermal operating point [T_{OP}, Fig. 20(c)]. At the intersection point, LG will be exactly -1 and the system will oscillate. The operation of this mode of sustained oscillations will be described by first assuming that $T < T_{\mathrm{OP}}$, that is, $\mathrm{ZE}_{\mathrm{CCFL}} > \mathrm{ZE}_{\mathrm{PT}}$. In this case, LG is smaller than -1 and, hence, the system is unstable which will cause the lamp current to build up. This will heat the lamp and reduce $\mathrm{ZE}_{\mathrm{CCFL}}$ (the local slope, $-R_s$, around the operating point in Fig. 16) moving the LG toward the $(-1, 0)$ point. When LG$= -1$ is reached the system will enter the sustained oscillation mode. The lamp rms current in this oscillatory mode $(I_{\mathrm{rms\_os}})$ is

$$I_{\mathrm{rms\_os}} = I_{\mathrm{rms\_s}}\sqrt{1+k^2} \tag{10}$$

where $I_{\mathrm{rms\_s}}$ is the lamp rms current at stable operation and k is the envelope AM modulation coefficient.

If the temperature moves to $T > T_{\mathrm{OP}}$, $|\mathrm{LG}| < 1$ [Fig. 20(c)], the system becomes stable and oscillations cease. In this case, the lamp current $(I_{\mathrm{rms\_s}})$ is lower than $I_{\mathrm{rms\_os}}$ (10). This will cause the lamp to cool down, $|\mathrm{ZE}_{\mathrm{CCFL}}|$ will increase Fig. 20(c) and the operating point will move back to the $(-1.\,0)$ point.

VIII. Conclusion

The envelope analysis concept was applied to investigate the thermal effects of PT–CCFL systems and to delineate their stability criterion. It was found that the main cause for instabilities is the fact that the EI of the PT includes a minimum point at low frequency when $f_m \cong |f_c - f_r|$. The EI of the CCFL was found to decrease with temperature, which makes the system less stable at lower temperature. This characteristic may cause the system to be unstable at one temperature and stable at a higher temperature. Sustained oscillations are observed when moderate instability are initially present and the oscillations heats up the lamp, $\mathrm{ZE}_{\mathrm{CCFL}}$ increases and the system enters the pseudo stable state of LG$= -1$.

The findings of this study help to better understand the behavior of PT–CCFL systems and will eventually help to develop methods for stabilizing the system under any desired operating condition.

References

[1] G. Spiazzi and S. Buso, "Small-signal analysis of cold cathode fluorescent lamp ballasts," in *Proc. IEEE Power Electron. Spec. Conf. (PESC'05)*, Recife, Brazil, 2005, pp. 2783–2789.

[2] S. Ben-Yaakov, M. M. Peretz, and S. Lineykin, "Stability of cold cathode fluorescent lamps driven by piezoelectric transformers," in *Proc. IEEE Appl. Power Electron. Conf. (APEC'06)*, Dallas, TX, 2006, pp. 1517–1522.

[3] S. Ben-Yaakov and G. Ivensky, "Drivers and rectifiers for piezoelectric elements," in *IEEE Power Electron. Spec. Conf. (PESC'05) Tutorial*, Recife, Brazil, 2005 [Online]. Available: http://www.ee.bgu.ac.il/~pel/public.htm#4

[4] C. D. Wey, T. L. Jong, and C. T. Pan, "Design and analysis of an SLPT-based CCFL driver," *IEEE Trans. Ind. Electron.*, vol. 50, no. 1, pp. 208–217, Feb. 2003.

[5] S. Glozman and S. Ben-Yaakov, "Dynamic interaction analysis of HF ballats and fluorescent lamps based on envelope simulation," *IEEE Trans. Ind. Appl.*, vol. 37, no. 5, pp. 1531–1536, Sep./Oct. 2001.

[6] E. Deng and S. C'uk, "Negative incremental impedance and stability of fluorescent lamp," in *Proc. IEEE Appl. Power Electron. Conf. (APEC'97)*, Atlanta, GA, 1997, pp. 1050–1056.

[7] S. Ben-Yaakov, S. Glozman, and R. Rabinovici, "Envelope simulation by SPICE-compatible models of linear electric circuits driven by modulated signals," *IEEE Trans. Ind. Appl.*, vol. 37, no. 2, pp. 527–533, Mar./Apr. 2001.

[8] S. Lineykin and S. Ben-Yaakov, "A unified SPICE compatible model for large and small signal envelope simulation of linear circuits excited by modulated signals," in *Proc. IEEE Power Electron. Spec. Conf. (PESC'03)*, Acapulco, Mexico, 2003, pp. 1205–1209.

[9] Y. Yin, R. Zane, J. Glaser, and R. W. Erickson, "Small-signal analysis of frequency based electronic ballasts," *IEEE Trans. Circuits Syst.*, vol. 50, no. 8, pp. 1103–1110, Aug. 2003.

[10] J. A. Oliver, C. Fernandez, R. Prieto, and S. A. Cobos, "Circuit oriented model of rectifiers for large signal envelope simulation," in *Proc. IEEE Power Electron. Spec. Conf. (PESC'05)*, Recife, Brazil, 2005, pp. 2771–2776.

[11] S. Ben-Yaakov, M. Shvartsas, and S. Glozman, "Statics and dynamics of fluorescent lamps operating at high frequency: Modeling and simulation," *IEEE Trans. Ind. Appl.*, vol. 38, no. 6, pp. 1486–1492, Nov./Dec. 2002.

[12] M. Gulko and S. Ben-Yaakov, "Current-sourcing parallel-resonance inverter (CS-PPRI): Theory and application as a discharge lamp driver," *IEEE Trans. Ind. Electron.*, vol. 451, no. 3, pp. 285–291, Jun. 1994.

[13] S. Ben-Yaakov and N. Krihely, "Modeling and driving piezoelectric resonant blade elements," in *Proc. IEEE Appl. Power Electron. Conf. (APEC'04)*, Anaheim, CA, 2004, pp. 1733–1739.

[14] S. Bronstein, "Piezoelectric Transformers in Power Electronics," Ph.D. thesis, Ben-Gurion Univ., Beer-Sheva, Israel, 2005.

[15] S. Ben-Yaakov and M. M. Peretz, "Simulation bits©: Some less familiar features of PSpice," *IEEE Power Electron. Soc. Newsl.*, pp. 16–18, 2005.

[16] *"PSpice Optimizer User's Guide,"* Cadence Design Systems, Inc., 2000.

[17] E. Deng, "Negative Incremental Impedance of Fluorescent Lamp," Ph.D. dissertation, California Inst. Technol., Pasadena, 1995.

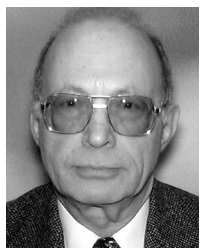

Shmuel (Sam) Ben-Yaakov (M'87) was born in Tel Aviv, Israel, in 1939. He received the B.Sc. degree in electrical engineering from the Technion, Haifa, Israel, in 1961 and the M.S. and Ph.D. degrees in engineering from the University of California, Los Angeles, in 1967 and 1970, respectively.

He is presently a Professor at the Department of Electrical and Computer Engineering, Ben-Gurion University of the Negev, Beer-Sheva, Israel, where he heads the Power Electronics Group. He was the Chairman of that Department from 1985 to 1989. He serves as Chief Scientist of Green Power Technologies, Ltd., Israel, and is a Consultant to commercial companies on various subjects, including analog circuit design and power electronics. His current research interests include power electronics, circuits and systems, electronic instrumentation, and engineering education.

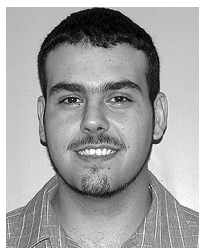

Mor Mordechai Peretz (S'06) was born in Beer-Sheva, Israel, in 1979. He received the B.Tech. degree in electrical engineering from the Negev Academic College of Engineering, Beer-Sheva, in 2003 and the M.Sc. degree in electrical and computer engineering from the Ben-Gurion University of the Negev, Israel, in 2005, where he is currently pursuing the Ph.D. degree.

His areas of interests include digital control, switch-mode dc–dc converters, modeling and computer aided design, lighting systems and ballasts, nonlinear magnetics, and resonant power conversion systems.